Dalton Transactions

Accepted Manuscript

ROYAL SOCIETY OF CHEMISTRY

www.rsc.org/dalton

Cite this: DOI: 10.1039/c0xx00000x

www.rsc.org/xxxxxx

ARTICLE TYPE

Water-soluble oxoglaucine-Y(III), Dy(III) complexes: In vitro and in vivo anticancer activity by triggering DNA damage, leading to S phase arrest and apoptosis

Jian-Hua Wei, Zhen-Feng Chen,* Jiao-Lan Qin, Yan-Cheng Liu, Zhu-Quan Li, Taj-Malook Khan, Meng Wang, Yan-Hua Jiang, Wen-Ying Shen and Hong Liang*

Received (in XXX, XXX) Xth XXXXXXXXX 20XX, Accepted Xth XXXXXXXXX 20XX
DOI: 10.1039/b000000x

Complexes of yttrium(III) and dysprosium(III) with traditional Chinese medicine active ingredient oxoglaucine (OG), $[Y(OG)_2(NO_3)_3]\cdot CH_3OH$ (**1**) and $[Dy(OG)_2(NO_3)_3]\cdot H_2O$ (**2**), were synthesized and characterized with elemental analysis, IR, ESI-MS, ^1H and ^{13}C NMR as well as single-crystal X-ray diffraction analysis. *In vitro*, the complexes exhibited higher anticancer activity than the free ligand OG against the tested cancer cell lines. Amount the tested cell lines, HepG2 is the most sensitive to the complexes. Complex **2** can trigger DNA damage in HepG2 cells, resulting in a cell cycle arrest in S phase and leading to cell apoptosis. The S phase cell-cycle arrest is caused *via* an ATM (ataxia-telangiectasia mutated)-Chk2-Cdc25A pathway. Chk2 is phosphorylated and activated in an ATM-dependent manner. It in turn phosphorylates Cdc25A phosphatise on serine124, causing the inactivation of Cdc25A in ubiquitin-mediated proteolytic degradation. The cyclin-Cdk complexes of S phase could also be inhibited by limited supply of cyclin A and E. This irreversible cell cycle arrest process ultimately induces mitochondria-involved apoptotic cell death *via* the activation of Bcl-2 protein. Complex **2** effectively inhibited tumour growth in the BEL-7402 xenograft mouse model, and exhibited higher safety *in vivo* than cisplatin.

Introduction

Anticancer metal complexes have attracted considerable interests since the successful application of platinum-based anticancer drugs.[1,2] Compared with the organic compounds, the metal complexes have a variety of coordination numbers and a higher structural diversity due to their geometries. Metal-containing compounds can also be designed as protein binders with particular properties of the involved metals.[3,4] Lanthanide(III) complex is another most promising anticancer metal complex and its antitumor activity is gradually being recognized. Recently, Che and co-workers reported a series of ytterbium(III) porphyrin complexes that show potential anti-cancer activities with IC_{50} values as low as sub-micromolar level. Ones of the ytterbium(III) complexes exerts its anticancer effect through inducing the apoptosis that is highly associated with endoplasmic reticulum stress pathway.[5] The lanthanide(III) complexes with the bioactive ligands of coumarins have anti-proliferative activity on various cancer cell lines.[6,7] The rare earth (III) nitrate with all-trans retinoic acid and L-glutamic acid possess different degrees of inhibiting effects on HepG2, A549 and HeLa cells. The suppression ratio of the complexes against the tested tumour cells is superior for the two ligands.[8] We previously reported that the lanthanide(III) complexes with halo-substituted 8-quinolinol displayed significant potency against a panel of cancer cell lines *via* interaction with DNA or induction of DNA cleavage.[9,10] However, the anticancer lanthanide(III) complexes are poorly water-soluble, which limits their development and application.

The main text of the article should appear here. Headings and subheadings should be formatted using the relevant button from the "Apply Style" dialog box (see the RSC Tools toolbar above).

Traditional Chinese medicine (TCMs) holds an important position in primary health care over vast rural areas of China, and it has been recently recognized by the world as a fertile source for revealing novel lead compounds for modern drug discovery.[11] It has been reported that some metal complexes with TCMs can afford novel potential (pro) anticancer effects.[12,13] In the recent years, our group has devoted to the synthesis of oxoaporphine−metal anticancer complexes, and reported a series of lanthanide(III) complexes bearing TCM active ingredient ligands as anticancer agents.[14,15] Oxoglaucine(OG) is an oxoaporphine alkaloid that is found in many TCMs, such as aquilegia ecalcarata Maxim (Ranunculaceae). It has been confirmed that OG possesses strong anticancer activity against HCT-8 (ED_{50}=2.85 μM) and KB (ED_{50}=5.69 μM).[16–18] However, anticancer mechanism of the lanthanide(III) complexes with oxoaporphine is still not well understood. In the present work, two water-soluble yttrium(III) and dysprosium(III) oxoglaucine complexes were prepared. The binding properties of the complexes to DNA were investigated by means of UV-visible

(UV-Vis) spectrometry, fluorescence microscopy, viscosemeter and agarose gel electrophoresis. The effects of the complexes on the expresses of apoptosis-related proteins and the cell cycle-related proteins were explored.

Results

Characterization of complexes 1 and 2

Oxoglaucine was synthesized as previously reported.[14] $[Y(OG)_2(NO_3)_3]\cdot CH_3OH$ (**1**) and $[Dy(OG)_2(NO_3)_3]\cdot H_2O$ (**2**) were synthesized by treating oxoglaucine respectively with $Y(NO_3)_3\cdot 6H_2O$ and $Dy(NO_3)_3\cdot 6H_2O$ in MeOH/$CHCl_3$ (4:1) under the solvothermal conditions. Both complexes were characterized using elemental analysis, infrared spectroscopy (IR) and electro-spray ionization mass spectrometry (ESI-MS), ^{1}H NMR and ^{13}C NMR spectroscopy. Their structures were determined with single-crystal X-ray crystallography diffraction analysis (Fig. 1, Supporting Information Figure S1). Both complexes **1** and **2** showed a mononuclear structure. The coordination geometry of the Y or Dy atom adopts bicapped tetragonal antiprism, which is ten coordinated by two N and two O atoms from the two bidentate OG ligands and six O atoms of the nitrates. The lengths of Y–O, Dy–O and Y–N, Dy–N bonds are in the ranges of 2.351–2.534 Å, 2.361–2.549 Å and 2.578–2.590 Å and 2.587–2.598 Å, respectively. The dihedral angles between the two OG planes in complexes **1** and **2** are 13.119º and 14.465º, respectively, suggesting that the complexes retain planarity. This feature is essential for their bioactivity.

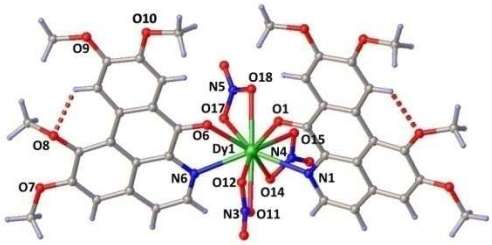

Fig. 1 Crystal structures of complex **2**

The mass spectra of complexes **1** and **2** in MeOH/H_2O (1:500) are presented in Figure S2 (see Supporting Information). A major peak (m/z 990.2) with a single isotope distribution was observed in the mass spectrum of complex **2**. It can be assigned to $[Dy(OG)_2(NO_3)_2]^+$, resulted from the loss of a NO_3^- anion from the complex. The divalent cationic peak m/z 639.8 is attributed to $[Dy(OG)_2(NO_3)+OG]^{2+}$, resulted from the loss of two NO_3^- anions and the combination with another OG molecule that occupies the vacant coordination site of the central metal ion. As expected, m/z 522.8 peak of $[Dy(OG)_2+2OG]^{3+}$ was found, which was resulted from the loss of three coordinated NO_3^- anions and the combination with two OG molecules. These results indicate that the three NO_3^- anions in the complex can easily be disassociated in a solution, consistent with our previous report that aqua ligands are easily lost during electrospray ionization process.[14] The formation of the cationic groups improves the water-solubility of the complexes to over of 7 mg mL^{-1} in aqueous solutions at room temperature and enhances the interaction between complexes and DNA.

The stabilities of complexes **1** and **2** in PBS solution (50 mM sodium phosphate, 4 mM sodium chloride, pH 7.4 at 25 °C) were determined using HPLC. No obvious changes in the HPLC chromatograms of the complexes in PBS solution were observed in 12 h, 24 h and 48 h (Supporting Information, Figure S3). In all, the complexes are stable in PBS solution over a 48h period at room temperature.

Contrasting subcellular distribution of complex 2

It has been confirmed that the distribution of metal complex in subcellular organelles is associated with different cellular pathways.[12,22,23] In the present work, complex **2** was selected to investigate the subcellular distribution of the lanthanide complexes since complexes **1** and **2** have similar chemical structure, anticancer activity and biological activity as shown in the subsequent cell cycle analysis and topoisomerase inhibition test. Cells were treated with 10 and 20 μM of complex **2** for 24 h. The distribution of Dy in four subcellular fractions including cytosolic fraction (total soluble proteins from cytoplasm), membrane fraction (membrane proteins, cellular organelles and organelles membranes), nuclear fraction (total nucleus soluble proteins and nuclear membrane proteins) and cytoskeletal fraction (total cellular insoluble proteins and genomic DNA) was determined (Fig.2).[24] High Dy accumulations were found in the membrane fraction (1015.4 ng with 10 μM and 1846.1 ng with 20 μM of complex **2**) and cytoskeletal fraction (766.0 ng with 10 μM and 1071.1 ng with 20 μM of complex **2**). For the two remaining fractions, the dysprosium contents ration dropped significantly. As mention above, genomic DNA was included in the cytoskeletal fraction, indicating that complex **2** may be have a targeting effect on DNA, which is a potential target molecule for metal anticancer complexes.[25]

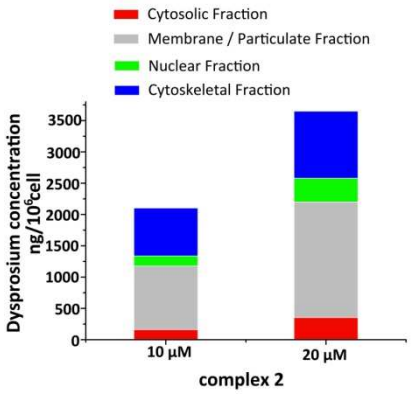

Fig. 2 Distribution of dysprosium in HepG2 cells that were exposed to 10 μM and 20 μM complex **2** for 24 h determined by ICP-MS.

Metal accumulation in nuclear DNA

To verify the hypothesis that DNA is the major target of the lanthanide complexes, HepG2 cells were treated with 10 and 20 μM of complex **2** and $Dy(NO_3)_3$ for 24 h. The nuclear DNA was isolated and its dysprosium content was examined with ICP-MS. As shown in Fig. 3, 1.43 ± 0.83 ng and 1.96 ± 0.74 ng dysprosium were detected in every one million HepG2 cells treated with 10 and 20 μM of $Dy(NO_3)_3$ respectively. In contrast, dysprosium contents in the DNA sample from cells treated with complex **2** are significantly higher and increase in a dose-dependent manner (4.92 ± 1.23 ng and 24.6 ± 1.94 ng,

respectively).

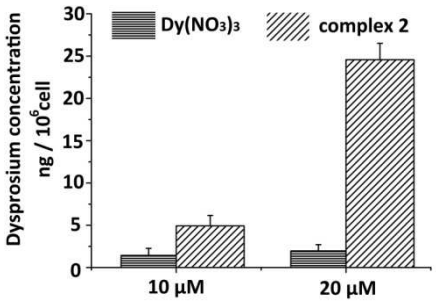

Fig. 3 Contents of dysprosium bound to the DNA of HepG2 cells treated with complex **2** and $Dy(NO_3)_3$.

Anticancer activity *in vitro*

The in vitro cytotoxicities of OG, complexes **1** and **2**, and corresponding metal salts against four cancer cell lines (T-24, HepG2, SK-OV-3, SK-OV-3/DDP) and two human normal cell lines (HL-7702, HUVEC) were screened using MTT assay with cisplatin as a positive control. The IC_{50} values toward the tested cell lines are summarized in Table 1.

Both complexes presented higher *in vitro* anticancer activity to all cell lines than free OG ligand and their corresponding metal salts. This might be caused by the synergistic effect of OG with the metal ions. Although complexes **1** and **2** showed slightly different IC_{50} values, both of them exhibited preferential anticancer activity toward HepG2 cells with IC_{50} values of 11.4±0.9 and 12.9±1.8 μM respectively. SK-OV-3/DDP is a cisplatin-resistant cell lines with a cisplatin IC_{50} of 85.9±1.3 μM.[26] It can be seen from Table 1 that the cell line is much more sensitive to OG, complexes **1** and **2** with IC_{50} values of 35.1±1.3, 28.3±2.3, 23.2±0.9 μM, respectively, suggesting that SK-OV-3/DDP cell line is not resistant to OG, complexes **1** and **2** under the same experimental conditions. This results also strongly suggest that the anticancer mechanisms of OG and metal-OG complexes are different from that of cisplatin. In addition, it can be concluded by comparing the IC_{50} values for cancer and normal cell lines that complexes **1** and **2** have remarkably higher antiproliferative efficiency toward the cancer cell lines than toward human normal cell lines HL-7702 and HUVEC. Thus, complexes **1** and **2** exhibit some extent cytotoxic selectivity to the tested cancer cell lines.

Table 1 IC_{50}[a] (μM) values for OG, complexes **1** and **2**, corresponding metal salt against six cell lines.

	T-24	HepG2	SK-OV-3	SK-OV-3/DDP	HUVEC	HL-7702
OG	43.7±2.5	28.0±1.1	46.1±1.0	35.1±1.3	90.2±1.3	40.2±1.0
Complex **1**	20.5± 3.5	11.4±0.9	18.0±1.5	28.3±2.3	62.1±1.2	37.8±0.9
Complex **2**	21.4 ± 1.0	12.9±1.8	29.4±1.0	23.2±0.9	75.6±0.7	43.0±1.0
$Y(NO_3)_3$	75.1±0.9	60.2±0.2	82.5±1.6	98.0±0.6	＞250	30.7±0.7
$Dy(NO_3)_3$	79.6±0.8	73.5±1.0	68.2±0.	86.7±1.9	＞250	32.6±0.6
Cisplatin [b]	7.4 ± 1.2	7.7±0.5	6.5±1.1	85.9±1.3	85.1±1.9	5.1±0.8

[a] IC_{50} values are presented as the mean ± SD (standard error of the mean) from five separated experiments. [b] 1 mM cisplatin in 0.154 M NaCl was used as a positive control.

Induction of cell cycle arrest

As both complexes **1** and **2** exhibit better growth inhibition on HepG2 cells, we investigated complexes **1** and **2**, corresponding metal salts and free ligand OG effects on cell cycle progression using flow cytometry in propidium iodide stained cells after treatment for 48 h.

Complexes **1** and **2** caused dose-dependent increases in their S phase arrests (Fig.4). With the increase of complexes concentration from 5 μM to 20 μM, the percentage of cells in S phase increased from 23.88% and 28.12% to 43.79% and 58.33%, respectively. In contrast, ($Y(NO_3)_3$, $Dy(NO_3)_3$), and OG showed no effect on HepG2 cell cycle at maximal concentrations (20 μM). As described above, dysprosium is highly accumulated in DNA samples when the cells were treated with complex **2**. Most DNA replication occurs within this stage. These suggest that the metals bind to DNA, may interfere with DNA replication, and thus cause the S phase arrest in HepG2 cell lines.[27, 28] To verify this hypothesis, Click-iT EdU assay was carried out to measure the ability of cells to complete DNA replication (Fig.5). EdU (5-ethynyl-2'-deoxyuridine) is a new nucleoside analog of thymidine that is incorporated into DNA during its replication.[29] In the control cell lines, EdU was incorporated into DNA (Green). When the cells were treated with 10 μM of complex **2** for 24 h, only slight green fluorescence was observed, indicating that complex **2** inhibited DNA replication process.

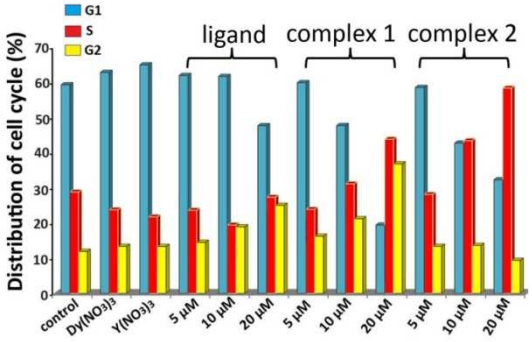

Fig. 4 Graph bar show the distributions at different portions of the cell cycle with treatment of metal salt, OG, complexes **1** and **2**, respectively.

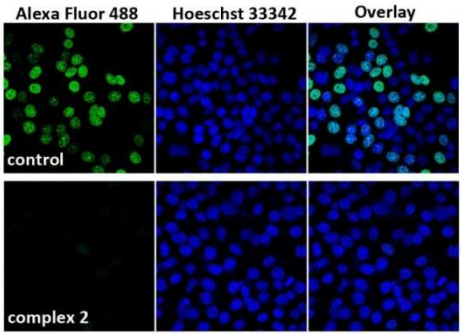

Fig.5 HepG2 cells were cultured with complex **2** at 10 μM for 24 h. Cells were labeled by EdU incorporation (Green).

The expression levels of some specific cell cycle-related proteins in the cells treated with and without complex **2** were determined using Western blot (Fig. 6). The expression levels of Cdk 2, Cdk 4 and Cdk 6 remained unchanged or slight changed, when the cells were treated with complex **2** for 48 h. In contrast, the expressions of cyclin A, cyclin B1 and cyclin E were reduced. Significantly, the complex **2** treatment caused time- and dose-dependent degradation in the expression of cyclin A and cyclin E. These results reveal that cyclin-Cdk complexes of S phase can be inhibited by limiting the supply of cyclin A2, E1.

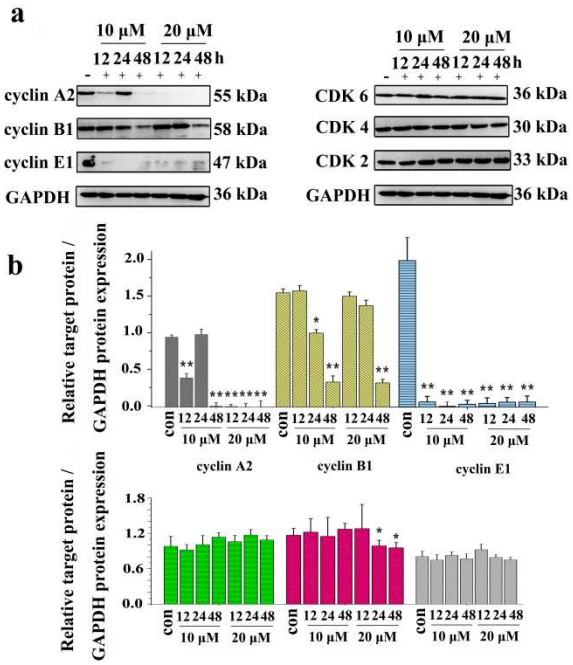

Fig. 6 (a) Effects of complex **2** treatment in HepG2 cells on cell cycle regulatory proteins at 10 μM and 20 μM for 12, 24, 48 h, respectively. (b) The relative expression of each band = (density of each band/density of actin band). Mean±SD was from three independent measurements. *p <0.05 and **p < 0.001.

Apoptosis

The annexin V-FITC/7-AAD assay was performed to determine whether the complexes-induced cell growth inhibition was the result of apoptosis. Exposure of HepG2 cells to different concentrations (5, 10, 20 μM) of complex **2** for 24 h resulted in a dose-dependent increase in the percentage of the early apoptotic tumour cells (Fig. 7) After the treatment of cells with 20 μM of complex **2**, the percentages of cells undergoing apoptosis and necrosis significantly increased to 60.4% and 13.8%, respectively. In contrast, similar treatments with 20 μM of $Dy(NO)_3$ and OG resulted in only a small amount of early apoptotic cells (0.79% and 1.78% respectively), which correlates with their ability to cellular uptake and their effects on cell cycle progression. Next, we sought the possibility that apoptosis was responsible for the antitumour action of the complexes. Apoptosis was assessed by measuring the number of nuclei positive to TUNEL labelling with a confocal microscopy. The findings show that untreated HepG2 cells were negative to TUNEL labelling and HepG2 cells treated with 10 μM complex **2** for 24 h were positive to the labeling. (see supporting information Figure S5). Consistent with the results was obtained in morphological analysis, the complex **2**-treated HepG2 cells were stained with DAPI (blue) and Did (red), morphological change to cell shrinkage, a phenomenon of apoptosis, and apoptosis bodies were observed in Fig.8.

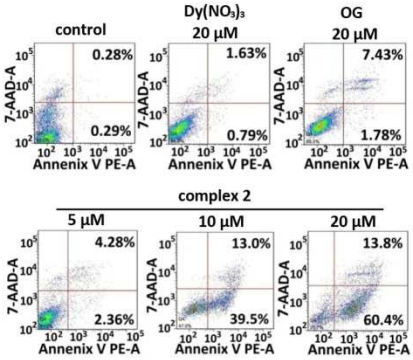

Fig.7 Induction of apoptosis by OG, $Dy(NO_3)_3$ and complex **2** in HepG2 cell lines. The cells were treated with the compounds for 24 h, and their apoptosis was determined using Annexin V/7-AAD staining with a flow cytometry. Annexin V (+) and 7-AAD (-) cells are labeled as early apoptotic cells, whereas Annexin V (+) and7-AAD (+) cells are labeled as late apoptotic cells.

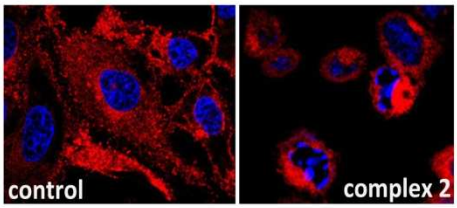

Fig. 8 Morphological analysis of the nucleus and the cell membrane in HepG2 cells treated with 10 μM complex **2** for 24 h on a confocal microscopy with a planapochromate 40×NA 1.52 oilimmersion objective.

The intrinsic pathway *via* mitochondria plays a key role in regulating apoptosis in response to various stimuli.[30] To further investigate the apoptotic pathway activated by complex **2**, the expression levels of a series of proteins related to the intrinsic mitochondrial were determined using Western blot. Bcl-2 family proteins are the key regulators of mitochondrial membrane potential. As shown in Fig.9, complex **2** down-regulated the expressions of anti-apoptotic protein Bcl-2 and Bcl-xL, and up-regulated the expressions of pro-apoptotic protein Bax and Bim. Furthermore, treatment of HepG2 cells with complex **2** under the same experimental conditions of the annexin V-FITC/7-AAD assay, caused a dose-dependent increase in the expression levels

of cleaved caspase-3 and cleaved poly(ADP-ribose) polymerase. These two proteins are another hallmark of apoptosis as it leads to cellular inactivation and prevents DNA repair cycles.[31] As expected, the up-regulation of cleaved caspase-9 and cytosolic cytochrome c were observed in response to treatment with complex **2** for 24 h. Thus, it can be concluded that HepG2 tumour cells undergo apoptosis *via* mitochondria-mediated pathway when they are treated with dysprosium (III)complex.[32]

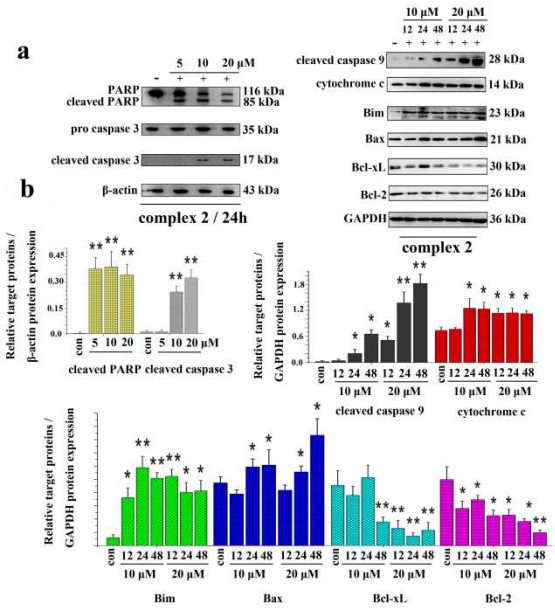

Fig. 9 Complex **2** regulate mitochohdria-mediated apoptosis proteins (a) Western blot analysis of caspase-3, cleaved caspase-3 and cleaved PARP after treatment of HepG2 cells with complex **2** at 5, 10, 20 μM respectively, for 24h; Western blot analysis the expression of a series of proteins involved in mitochondria-mediated apoptosis after treatment with complex **2** at the indicated concentration and for the indicated times.(b) Western blotting bands from three independent measurements, the relative expression of each band = (density of each band/density of actin band). *p <0.05 and **p < 0.001.

DNA binding properties of the compounds

It has been reported that metal complexes can mediate apoptosis through DNA damage[33] As discussed above, complex **2** can induce S phase arrest *via* interfering DNA replication. Here the binding properties of OG and complex **2** to DNA were explored using fluorescence microscope, viscosity measurement, and agarose gel electrophoresis. These investigations could provide direct evidences for apoptosis induced by DNA damage mediated S-phase arrest. GelRed (GR) was chosen as an environmentally safe and ultra-sensitive DNA intercalative fluorescence probe to investigate the binding abilities of compounds to ct-DNA.[34] As shown in Fig.10, compared with OG that did not decrease the flurescence emission intensity of GR; complex **2** can effectively quench the fluorescence emission of GR. When the [complex] / [DNA] / [GR] ratio increased to 1:10:7 upon the addition of complex **2**, the fluorescence emission intensity of GR was decreased to 41.7% of the original intensity. These results strongly suggest that complex **2** competes with GR in binding to DNA.[35] The quenching constants (K_q) of OG and complex **2** were calculated using Stern−Volmer quenching equation as 1.1×10^3 and 7.6×10^4, respectively.(see supporting information Figure S6) Hence, it can be concluded that complex **2** has a higher intercalative binding affinity to DNA than free OG ligand. The higher binding affinity might be attributed to the electrostatic interaction between central metal cations and DNA.[36]

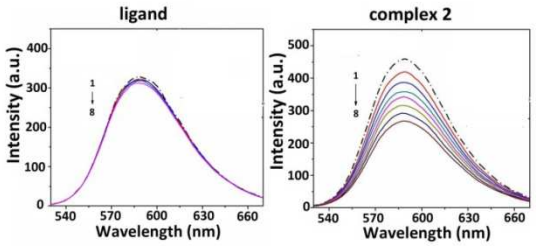

Fig.10 Fluorescence emission spectra of the GelRed bound to DNA ([DNA] = 2.0×10^{-4} M, [GelRed] = 2.0×10^{-5} M) in the absence (dashed line ---) and in the presence (solid lines —) of OG and complex **2** at [compound]/[GelRed] ratios range from 1:1 to 9:1. Inset: linear fitting for quenching constant Kq based on Stern-Volmer equation.

The viscosity of DNA was used as another parameter to compare the binding abilities of tested compounds to DNA. Fig.11 is the relative viscosity of salmon sperms DNA treated with complex **2**, OG, ethidium bromide (EB) and Hoechst33258. The addition of each compound with [compound]/[DNA] ratios ranging from 0.01 to 0.10 led to the increment on the viscosity of ss-DNA solution in different extents. By contrast, the addition of complex **2** increased the viscosity more effectively than OG. The increment on the DNA viscosity by complex **2** was even higher than the classic intercalator, EB, at the [compound]/[DNA] ratios lower than 0.08. Finally, at the [compound]/[DNA] ratio of 0.10, the increment on the DNA viscosity represented as $(\eta/\eta^0)^{1/3}$ increased to 1.06, 1.05 and 1.04 by EB, complex **2** and OG, respectively. In contrast, the relative viscosity of DNA treated with Hoechst33258 remained unchanged in the whole ratio range, which was served as a minor groove binder. These results suggest that complex **2** intercalatively bind to DNA due to the aromatic planar structure of OG. The central lanthanide(III) ion may also facilitate the interaction between the complex and DNA through exterior electrostatic attraction, which resulted in the higher binding affinity of complex **2** to DNA.[37]

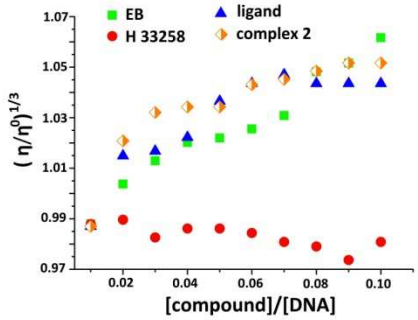

Fig.11 Relative viscosity changes of 1 mM Salmon sperm DNA from the cells treated with OG and complex **2** at [compound]/[DNA] ratios ranging from 0.01 to 0.10.

To further confirm the electrostatic interaction between metal complexes and DNA, Sodium dodecyl sulfate (SDS) was selected as a probe to investigate the electrostatic interaction between complex **2** and DNA, due to the dodecyl sulfate anion acts as an

appropriate substitute for DNA polyanionic backbone, which could be monitored by UV-Vis absorption spectroscopy. As shown in Fig.12, the intensity of the complex **2** absorption spectra in the presence of SDS was significantly decreased with the increase of SDS concentration. In contrast, the intensity of OG absorption spectra was slightly decreased in the presence of SDS. Thus, in addition to intercalation, the electrostatic interaction between the cationic complex and the polyanionic DNA alphosphate backbone also contributes the binding ability of the complex to DNA. This is consistent with the results of competitive binding experiments as described above.[38]

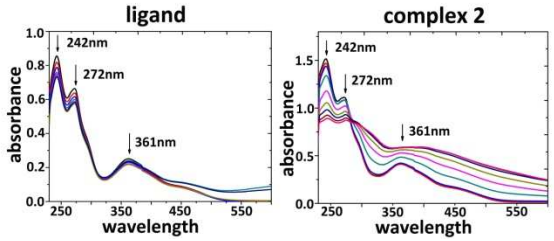

Fig.12 UV-Vis absorption spectra of complex **2** and OG in the absence (black line) and in the presence of various amounts of SDS (0-3×10-4 mol/L) at room temperature.

Gel electrophoresis of pBR322 plasmid DNA was carried out to determine its shift mobility in the presence of OG and complex **2**. As shown in Fig.13, the electrophoresis mobility of supercoiled DNA was decreased with the increasing concentrations of OG and complex **2** from 20 μM to 100 μM. This is attributed to the intercalation of the neighbouring base pairs of OG or complexes into the DNA chain.[39] It is noticeable that the presence of 100 μM complex **2** caused half amount of Sc DNA degraded into relaxed form DNA (R DNA). The results indicate the metal complex can cleave Sc DNA, in which the coordinated metal plays key roles.[40]

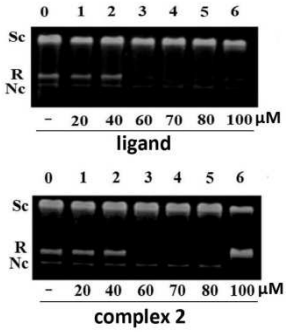

Fig. 13 Gel electrophoresis mobility shift assay of pBR322 DNA treated with OG and complex **2** (lane 0: DNA alone; lanes 1-6: DNA + OG or complex **2**, with increasing concentrations of 20, 40, 60, 70, 80 100 μM, respectively). R: linear form DNA, Sc: supercoiled form DNA, Nc: circular form DNA.

Based on the DNA cleavage ability of the complex **2**, we hypothesize that it can induce DNA damage, cause a series of signal transductions, and eventually result in cell cycle arrest and apoptosis. As shown in Fig.14, both ATM and Chk2 were activated when the cells were treated with complex **2**. In addition, complex **2** caused the down-regulation of total Cdc25A, and up-regulation of the serine124 of Cdc25A, which is required for the phosphorylation of Chk2 during the $SCF^{\beta TRCP}$ – dependent degradation of Cdc25A in S-phase.[41] The inactivation of total Cdc25A results in the accumulation of phosphorylated Cdk2 on Tyr 15 (inactive form), which is incapable of initiating DNA replication.[42] Moreover, the hyperphosphorylation on Tyr 15 of Cdk2 also cause the inhibition of the cyclin-Cdks complexes. These results indicate Chk2 is a mediator to destruct Cdc25A in response to the lanthanide complex-induced DNA damage with S-phase checkpoint.

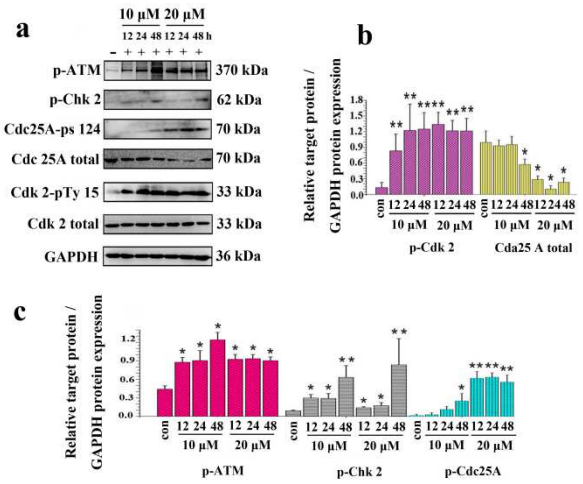

Fig. 14 Complex **2** activates the ATM-Chk2-Cdc25A pathway. (a) Western blot analysis of the inductive effect of complex 2 on the expression levels of the proteins involved in the ATM-Chk2-Cdc25A pathway. (b,c) The relative expression of each band = (density of each band/density of actin band). Mean±SD was from three independent measurements. *p <0.05 and **p < 0.001.

Inhibition of Topoisomerase I

Topoisomerases (I and II) are essential nuclear enzymes to maintain the topological changes of DNA and to complete DNA transcription, replication and chromosome segregation.[43] Camptothecin and its derivative are well-known topoisomerase I (Topo I) inhibitors, which induce apoptotic pathways by binding to and stabilizing the topoisomerase I-DNA complex and thus inhibit DNA re-ligation. It can induce both single strand breaks (SSBs) and double strand breaks (DSBs), ultimately, leading to severe DNA damage response and activation of DNA damage-related molecules, such as ATM / ATR.[44] We have previously reported that the oxoaporphine transition metal complexes can inhibit the activity of topoisomerase I.[45] Here, the inhibition of Topo 1 activity by the lanthanide(III) complexes was tested using DNA relaxation assay to explore if it is related to the cytotoxicity of the complexes and the complex-inducing DNA damage.

The DNA relaxation assay was carried out with camptothecin (CPT) as a positive control.[46,47] When the complex was added to the mixture of Topo I and pBR322 DNA plasmid, no obvious change was observed in the activity of Topo I (Fig.15a). In another assay, Topo I was pre-incubated with the compounds before the addition of plasmid pBR322 DNA. As show Fig. 15b upper panel, both complexes **1** and **2** started the inhibition of Topo I activity at 50 μM. In contrast, 80 μM OG only showed slight inhibition of Topo I activity. OG exhibited higher inhibitory activity when the incubation time was prolonged to 60 min. The complexes exhibited lower inhibitory activity when the DNA plasmid was pretreated with complexes (Fig.15c). It may be

explained that the pre-incubation of the compounds with DNA reduce the available amount of the complexes to inhibit Topo I activity. These results indicate that both DNA and Topo I are the potential binding targets of these compounds. Moreover, the different inhibition activities of complexes and OG towards Topo I may be another reason that complexes **1** and **2** are more cytotoxic than OG. Additionally, the inhibited Topo I activity could also accelerate the complex-induced DNA damage.

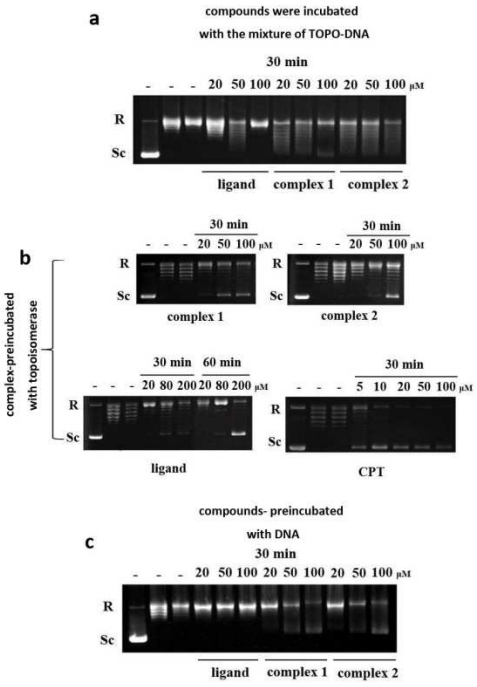

Fig. 15 Compounds inhibit the activity of Topoisomerase I. (a) Compounds was added to the mixture of Topo I and pBR322 DNA. (b) Inhibition of TopoI –mediated DNA relaxation by complexes **1**, **2**, OG and CPT, respectively. Lane 1, pBR322 DNA only; Lane 2, pBR322 DNA + Topo I; Lane 3, pBR322 DNA + TopoI + 5% DMSO; (c) Effect of preincubation of pBR322 DNA with OG, complexes **1** and **2**. Lane 1, pBR322 DNA only. Lane 2, pBR322 DNA + Topo I. Lane 3, pBR322 DNA + TopoI + 5% DMSO.

Human hepatocarcinoma xenograft growth inhibition in vivo

The acute toxicity of complex **2** was assessed over 14 days by treated with complex **2** at four dose (500/400/300/150mg/kg) by single injection(ip). Treated with complex **2** at dose of 300mg/kg killed one animal (Fig. 16a), this dose was take as the Maximum Tolerated Dose (MTD).

Another 4 groups animals (n=6) were used to evaluate the safety of complex **2**, treated with complex **2** at dose of 150, 75, 37.5 mg/kg daily by intraperitoneal injection for 10 day. As shown in Fig. 16b, 75 mg/kg was taken as the high dose *in vivo* anticancer studies.

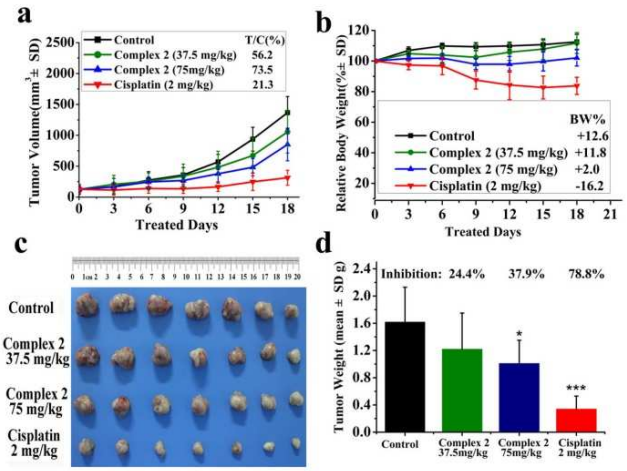

Fig. 16 *In vivo* anticancer activity of complex **2** in mice bearing BEL-7402xenograft. (a) Effect of complex **2** (37.5, 75 mg/kg/d), cisplatin (2 mg/kg/2 days), or vehicle (saline) on growth of tumour xenograft. Tumour growth is tracked by the mean tumour volume (mm^3)±SD (n=7) and calculated as the relative tumour increment rate (T/C, %). (b) Body weight change (presented as %change from initial weight). (c) Photographs of tumour from treatment groups and vehicle group. (d) Tumour weight was recorded after the mice were killed. (***) P<0.001,(*)P<0.05, p vs vehicle control.

The anticancer efficacy of complex **2** was shown in Fig. 16. The tumour-bearing nude mice were treated with 75 mg/kg and 37.5 mg/kg of complex **2** every day, a dose-dependent inhibition of relative tumour increment rate (T/C) showing 56.2% ($p<0.05$) and 73.5%, respectively. Cisplatin at 2 mg/kg (ip, q2d) controlled the tumour volume at 315 mm^3, indicating a T/C of 21.3% ($p<0.01$) inhibition of tumour growth. These suggested that complex **2** exhibited antitumour activity in BEL-7402 model (37.8%, $p<0.05$), but lower than cisplatin (78.8%, $p<0.001$).

It is worthwhile to note that toxic effects of complex **2** were not observed during the treatment. The average body weight of the mice treated with high dose (75 mg/kg) was 20.6 ± 0.5 g before and 21.0 ± 1.4 g after the therapy, and there is slight body weight loss in the low dose (37.5 mg/kg). However, the mice received cisplatin had an obviously body loss (Fig. 16b).

Discussion

It has long been recognized that the aporphine alkaloids represent widespread class of compounds. Oxoglaucine (OG) is oxoaporphine alkaloids which possess planar hydrophobic π conjugated systems, nitrogen and carbonyl, this special chemical structure give them a broad range of biological activities, including antimicrobial, antiviral, cytotoxic, etc. The developing of the metal-based anticancer drugs is attracting more and more person's attention.

In the present work, we synthesized two new water-soluble yttrium(III) and dysprosium(III) oxoglaucine complexes. Both complexes were found to exhibit promising anti-cancer activity with low cytotoxic IC_{50} values against HepG2 cell line. With regard to normal liver cell HL-7702, complexes **1** and **2** exerted lower toxicity than cisplatin. Compared with corresponding metal salts and ligand, complexes exhibit higher cytotoxic activities.

This result is consistent with the experimental observation that more Dy was bound to DNA in the cells treated with complex **2** than in the cells treated with $Dy(NO_3)_3$. In addition, intermediate lipophilic and hydrophilic properties are important for the toxicity, which can improve the toxicity of complexes by finding a balance between cell uptake and binding to extracellular proteins.[11,48] In our research, the mass spectra and HPLC spectra of complexes **1** and **2** showed that the three NO_3^- anions easily be disassociated, leading to the formation of the cationic group in the solution, which could improve the aqueous solubility of complexes. In contrast, the OG ligand might increase the lipophilicity of the complex and thus facilitate the transport of the complex **2** across cellular phospholipid membranes.[49] This consistent with the recent report that the ligand in a complex can not only enhance cell uptake, but also improve anticancer properties of metallic complexes.[50] It has been also reported that lipophilic metal complex cations show promising cytotoxicity to cancer cells both under in vitro and in vivo conditions.[51]

Many cancer chemotherapy drugs can directly or indirectly induce DNA damage, which is recognized by DNA damage checkpoint in the cancer cells.[52] It is therefore important to investigate the link between DNA damage and cell cycle/apoptosis, in order to facilitate our understanding of the molecular mechanism of antiproliferation induced by complexes. Different DNA lesions activate all checkpoints have similar functional components that include early damage sensors, PIKK kinases (ATM, ATR, and DNA-PK), mediator or signal transducer proteins (Chk1 and Chk2 signaling kinases), and effector proteins (phosphatases Cdc25A/B/C and cyclin-dependent kinases Cdks). It follows that DNA damage is first recognized and then signals are transmitted to cell cycle/apoptosis machinery.[42] Here, we observed that complex **2** can induce DNA damage by cleaving DNA as well as may act as topoisomerase I inhibitor, which do not stabilize Topo I-DNA cleavage complex (Topo I cc) but are equally able to inhibit the enzyme activity,[53] rather than topoisomerase I poisons, which prevent the religation step by stabilization of Topo I-DNA cleavable complexes.[54] DNA damage signal is sensed by the ATM (ataxia-telangiectasia mutated)-Chk2-Cdc25A pathway, causing the proliferation arrest in S phase. On the other hand, due to the limiting of cyclin A/E supply, cyclin A-Cdk 2 and cyclin E-Cdk2 complexes lose their regulation function in S phase.

In cell distributions studies, the data showed that complex **2** accumulate highly in the membrane fraction that includes the mitochondria membrane. Mitochondrial outer membrane permeabilization is considered the ''point of no return'' for apoptotic cell death, triggering release of pro-apoptotic factors such as cytochrome c and apoptosis-inducing factor.[55,56] In our present work, the DNA damage signal initiates Bcl-2 protein family, which maybe participate in the formation of pores in the outer mitochondrial membrane through which cytochrome C escape, leading to the activation of caspase 3, 9, and then cleavage of their specific substrate PARP. HepG2 tumour cells eventually undergo apoptosis via mitochondria-mediated pathway. Complex **2** possesses anticancer efficacy in the BEL-7402 xenograft mouse model, but lower than cisplatin. Meanwhile complex **2** has lower toxicity in vivo than cisplatin which was apparently as evidenced by loss of body weight compared to vehicle control.

In conclusion, this study demonstrates that two water-soluble lanthanide(III) complexes with the TCM active component oxoglaucine as a new class of metal-based anti-cancer agents. The complexes exhibit the anticancer activity in vitro and vivo, and exhibited higher safety in vivo than cisplatin. The flow cytometric analysis shows that complexes **1** and **2** exhibit effective cell growth inhibition by triggering S phase arrest and inducing apoptosis through mitochondria-mediated pathway.

Experimental Section

Chemicals, cells and materials

Unless otherwise stated, all the chemicals were purchased from Sigma and Alfa Aesar. And all chemical reagents including metal salts and solvents were used of analytical grade. Oxoglaucine (OG) was synthesized according to procedures described previously.

Synthesis and characterization of the complexes

$[Y(OG)_2(NO_3)_3]\cdot CH_3OH$ (**1**): OG (0.05 mmol, 0.018 g), $Y(NO_3)_3\cdot 6H_2O$ (0.1 mmol, 0.038 g), methanol (1 mL), chloroform (0.25 mL) were placed in a thick Pyrex tube (ca 20 cm long). The mixture was frozen by liquid N_2, evacuated under vacuum and sealed. Then it was heated at 80 °C for 72 h. Dark red block crystals suitable for X-ray diffraction analysis were harvested (Yield: 65%). ^{1}H NMR (600 MHz, DMSO-d_6) δ 8.83 (d, J = 5.0 Hz, 1H), 8.70 (s, 1H), 8.07 (d, J = 4.9 Hz, 1H), 7.77 (s, 1H), 7.66 (s, 1H), 4.07 (s, 3H), 4.02 (s, 3H), 3.99 (s, 3H), 3.94 (s, 3H). ^{13}C NMR (151 MHz, DMSO-d_6) δ 180.44 (s), 157.01 (s), 154.09 (s), 151.64 (s), 149.63 (s), 144.64 (s), 135.71 (s), 129.09 (s), 126.38 (s), 124.49 (s), 121.28 (s), 118.72 (s), 110.52 (s), 109.43 (s), 107.77 (s), 60.87 (s), 56.93 (s), 56.13 (s), 55.99 (s). IR (KBr, cm^{-1}): ν(–OH) 3420 (vs), ν(Ar–H) 2940 (m), ν(C=O) 1605(m), ν(C=C) 1574 1509 1473 (m), ν(N–O) 1384 (vs), ν(C–O) 1280 1257, ν(C–N) 1008(m). ESI-MS(in MeOH/H_2O): m/z=915.09 $[Y(OG)_2(NO_3)_2]^+$, m/z=602.11 $[Y(OG)_2(NO_3)+OG]^{2+}$, m/z=497.78 $[Y(OG)_2+2OG]^{3+}$. Calcd. for $C_{41}H_{38}N_5O_{20}Y$ (%): C, 48.77; H, 3.79; N, 6.94. Found: C, 48.83; H, 3.67; N, 6.89.

$[Dy(OG)_2(NO_3)_3]\cdot H_2O$ (2): OG (0.05 mmol，0.018 g), $Dy(NO_3)_3\cdot 6H_2O$ (0.1 mmol，0.038 g), methanol (1 mL), chloroform (0.25 mL) were placed in a thick Pyrex tube (ca 20 cm long). The mixture was frozen by liquid N_2, evacuated under vacuum and sealed. Then it was heated at 80 °C for 72 h. Dark red block crystals suitable for X-ray diffraction analysis were harvested (Yield: 70%). IR(KBr, cm^{-1}): ν(–OH) 3395 (vs), ν(Ar–H) 2939 (m), ν(C=O) 1605(m), ν(C=C) 1571 1508 1473(m), ν(N–O) 1314(vs), ν(C–O)1280 1253, ν(C–N) 1025(m). ESI-MS(in MeOH/H_2O): m/z=990.2 $[Dy(OG)_2(NO_3)_2]^+$, m/z=639.8 $[Dy(OG)_2(NO_3)+OG]^{2+}$, m/z=522.8 $[Dy(OG)_2+2OG]^{3+}$. Calcd. for $C_{40}H_{36}N_5O_{20}Dy$ (%): C, 44.93; H, 3.39; N, 6.55. Found: C, 50.01; H, 3.42; N, 6.51.

X-ray crystallography

The data for complexes **1** and **2** were collected on a SuperNova CCD area detector equipped with graphite monochromated Mo-Kα radiation (λ = 0.71073 Å). The structures were solved with direct methods and refined using SHELX-97 program. The non-

hydrogen atoms were located in successive difference Fourier synthesis. The final refinement was performed by full-matrix least-squares methods with anisotropic thermal parameters for non-hydrogen atoms on F^2. The hydrogen atoms were added theoretically, riding on the concerned atoms. The crystallographic data and refinement details of the structure analyses are summarized in Supporting Information, Table S1; the CCDC reference numbers are 1009609, 1009610 for complexes **1** and **2**.

Metal distribution in HepG2 cells

The cells were seeded in Petri dish. After 24 h of pre-incubation time in drug-free medium at 37 °C in a humidified atmosphere of 5% CO_2/95% air, the complex **2** were added to give final concentrations at 10, 20 μM. After a further 24 h of drug exposure, cells pellets were fractionated using the FractionPREP kit from BioVision according to the supplier's instructions. Each sample (including cytosol, nucleus, membrane/particulate and cytoskeletal fractions) was digested with HNO_3, the resulting solutions were diluted with double-distilled water to a final concentration of 5% HNO_3 (5mL), and the dysprosium(III) contents was determined by plasma-mass spectrometry (ICP-MS). Data is the mean of three experiments and reported as mean ± SD.

Anticancer activity assay *in vitro*

Human cancer cell lines T-24, HepG2, BEL-7702，SK-OV-3, and human umbilical endothelial cell HUVEC, were purchased from ATCC (Manassas, VA), and human normal liver cell HL-7702 and SK-OV-3/DDP were obtained from the Shanghai Cell Bank of the Chinese Academy of Sciences. Cisplatin was selected as a reference metallodrug in order to investigate the potency of these synthetic complexes. Cells were seeded in 96-well plates and treated with after one day with a range of corresponding compounds concentrations (1.25, 2.5, 5, 10, 20 μg/mL, respectively) for 48h. Anticancer activity screening by 3-(4,5-dimethylthiazol-2-yl)-2,5-diphenyltetrazolium bromide (MTT) assay was carried out. At the end of each incubation period, the MTT solution (10 μL, 5 mg/mL) was added into each well and the cultures were incubated further for 48 h. After removal of the supernatant, DMSO (150 μL) was added to dissolve the formazan crystals. The absorbance was read by enzyme labelling instrument with 570/630 nm double wavelength measurement. The anticancer activity was evaluated based on the percentage of cell survival in a dose-dependent manner relative to the negative control. The final IC_{50} values were calculated by the SPSS19.0. All tests were repeated in at least three independent trials.

Flow cytometric analysis

HepG2 cells were incubated in 10% FBS-supplemented culture medium with $Y(NO_3)_3$, $Dy(NO_3)_3$ at 20μM and with OG, complexes **1** and **2** at 5, 10, 20 μM for 48 h. After treatment, cells were collected and fixed with ice-cold 70% ethanol at −20ºC overnight. Fixed cells were resuspended in 0.5 mL of PBS containing 50 μg / mL propidium iodine, 100 μg / mL RNase A. The cell cycle distribution was analyzed by FACS Calibur flow cytometer (BD) and calculated using ModFIT LT software (BD).

HepG2 cells plated at 1×10^5 cells/mL in 6-well plates. Cells were then incubated with complete medium only (control), medium with OG, $Dy(NO_3)_3$ at 20μM , and with complex **2** at 5, 10, 20 μM respectively. After incubation for 24 h, the cell was trypsinized and collected. Induced apoptotic was assayed by the BD Pharmingen FITC Annexin V Apoptosis Detection kit, according to the manufacture's instructions.

EdU incorporation assay

HepG2 cells were grown on coverslips and treated with 10 μM complex **2** for 48 h and added 10 μM EdU into medium for 2 h incubation. After fixation, permabilization, Click-iTTM EdU Alexa Fluor® 488 Imaging Kit (Invitrogen) was used for staining. H33342 (1:2000) in PBS was added in the absence of light for 30 min and washed twice with PBS. The treated-coverslips were photographed with a Zeiss LSM710 confocal microscopy using a planapochromate 40×NA 1.52 oilimmersion objective.

TUNEL assay

The cancer cells (HepG2) were cultured on coverslips. Complex **2** (10 μM) was added to the culture medium (10% FBS, Gibco). The sample in the absence of the complex was used as negative control. After 24 h incubation, cells were treated with blocking, fixation and permeabilization solution, In Situ Cell Death Detection Kit (Roche) was used for staining for 30 min at room temperature, and then photographed with a Zeiss LSM710 confocal microscopy using a planapochromate 40×NA 1.52 oilimmersion objective.

Live Cell Confocal Microscopy

HepG2 cells were grown on chamber slides to 70% confluence. Complex **2** (10 μM) was added to the culture medium (final DMSO concentration, 5% v/v) and incubated for 24 h at 37 ºC. The cells were then washed with PBS, stained with medium containing DAPI/DiD solution (100 μg/mL DAPI, 100 μg/mL DiD) for 30 min. The cells were observed under Zeiss LSM710 confocal microscopy.

Spectroscopic studies on DNA interaction

The DNA-binding experiments were performed at room temperature, all spectroscopic experiments were carried out in TBS buffer. The synthetic compounds were prepared as 2.0 mM DMSO stock solutions, and the 2.0 mM ct-DNA stock solution was stored at 4 °C for no more than 5 days before use. In GelRed-DNA-compound ternary competitive binding studies, 2.5 mL solution containing 2×10^{-4} M DNA and 2×10^{-5} M GelRed ([DNA]/[GelRed] = 10:1) was prepared. Each compound was added into the above solution with increasing concentrations. Fluorescence emission spectra were recorded with slit width of 3 nm for Ex and 5 nm for E_m, respectively. The quenching constant K_q of each compound was obtained by the linear fit of plotting I_0/I versus [Q], according to the classic Stern–Volmer equation: $I_0/I = 1+K_q\times[Q]$, where I_0 and I are the peak emission intensity of the GelRed-DNA system in the absence and presence of each compound as the quencher, and [Q] is the concentration of quencher. In DNA viscosity measurements, ss-DNA was dissolved in BPE buffer (6 mM Na_2HPO_4, 2 mM NaH_2PO_4, 1 mM Na_2EDTA, pH=7.2) to prepare a 23 mL working solution of 1.0×10^{-3} M ss-DNA. Each compound was added with increasing concentrations to give the [compound]/[DNA] ratios ranging

from 0.01 to 0.10 in every 0.01 interval. Circulating bath temperature was maintained at 35.0 ± 0.1 °C. Data were presented as η/η^0 versus [compound]/ [DNA] ratio, in which η^0 and η refer to the viscosity of each DNA working solution in the absence and presence of the corresponding compound, respectively. In UV-Vis absorption spectrometry, sodium dodecyl sulfate (SDS) was dissolved in double distilled water, 2.5 mL solution containing 3×10^{-5} M OG/complex **2**. SDS was added into the above solution with increasing concentrations ($0–3\times10^{-4}$ mol/L). All DNA binding studies were based on repeated experiments.

Agarose gel electrophoresis assay

For plasmid DNA unwinding experiments, supercoiled pBR322 DNA(0.5 μg) was treated with different concentration of compounds in the TBE buffer (TBE: Tris-Boricacid-EDTA buffer solution), and the solution were incubated at 37 °C in dark for 4 h. The samples were analyzed by electrophoresis for 2 h at 70 V in the TBE buffer. The gel was then stained by EB for 20 min and visualized and photographed via a BIO-RAD imaging system under a UV-Vis transilluminator.

Western blotting

HepG2 cells (5×10^5) were cultured on 60 mm dish and incubated overnight before experiments, which were treated with corresponding concentration and time. After incubation, cells were harvested and lysed using the lysis buffer (150 mM NaCl, 100 mM Tris-HCl, pH 7.4, 10% glycerol, 1% Triton X-100, 10 mM NaF, 5 mM sodium pyrophosphate, 5 mM sodium orthovanadate, 0.1% SDS) with protease inhibitor. Total protein extracts (50 μg) were loaded onto suitable concentration SDS-polyacrylamide gel, and were then transferred to polyvinylidene fluoride (PVDF) membranes. The membrane was blocked with 5% BSA in TBST buffer and incubated with corresponding primary antibodies at 4 ºC overnight, cleaved caspase-3 (ab32042) (1:500), cleaved caspase-9 (ab32539) (1:500), Bax (ab32503) (1:2000), Bcl-2 (ab32124) (1:2000), Bcl-xL (54H6) (1:1000), Bim (1:1000), ATM (pS1981) (1:1000), Chk 2 phospho (pT68) (1:1000), Cdk2 phospho (pY15) (1:1000), Cytochrome C (3895-1) (1:1000), Cdc25A phosphor (ps124) (1:1000), were obtained from Abcam; Cyclin A2 (BF683) (1:1000), Cyclin B (V152) (1:1000), Cyclin E1 (HE12), (1:1000), Cdk2 (78B2) (1:1000), Cdk4 (DCS156) (1:1000), Cdk6 (DCS83) (1:1000), Cdc25A (1:500), were obtained from CST. After washing, the membrane was incubated with secondary antibody conjugated with horseradish peroxidase (1:2500) for 120 min. The immuno reactive signals were detected using enhanced chemoluminance kit (Pierce ECL Western Blotting Substrate) following the procedures given in the user manual.

In vivo anticancer activity

KM mice (both male and female, 20–22g, 5–6 weeks) and BALB /c nude mice (male, 20–22 g, 6–7 weeks old) were supplied by B eijing HFK Bioscience.co., LTD (Beijing, China, Approval No. S CXK 2014-004), and used for the human hepatocarcinoma (BEL-7402) xenograft. The vivo studies were carried out at the Institute of Radiation Medicine Chinese Academy of Medical Sciences (Tian Jin, China, Approval No. SYXK 2014–0002). All animal experiments followed ethical standards. Six-week old both KM mice (weight 20–22 g) were randomly divided into 4 groups (n=6) and treated with complex **2** at four dose (500/400/300/150mg/kg) by single intraperitoneal (ip) injection, the mice were observed for 14 days and the death of them was calculated. Considering the toxicity in multiple dosing, another 4 groups animals (n=6) were used to evaluate the safety of complex **2**, treated with **2** at dose of 150, 75, 37.5 mg/kg daily by intraperitoneal injection for 10 day, the signs of toxicity were observed and body weight was recorded every day.

Nude mice received subcutaneous injection of BEL-7402 at 5×10^7 cells in right flank. When the xenograft tumour growth to the volume about 1000 mm^3, the mice were killed and the tumourtissue were cut into about 1.5 mm^3 small pieces, and then transplanted into the right flank of male nude mice. When the average tumours reach a volume of 100～150 mm^3, the mice were randomized into solvent control and treatment groups (n=7/group). Complex **2** at doses of 75 and 37.5 mg/kg (dissolve in saline) were given every day for 17 days (ip), cisplatin at doses of 2 mg/kg/per two days and control mice received the solvent (saline). Tumour volume and inhibition of tumour growth were calculated using formulas 1, 2 and 3:[19–21]

Tumour volume: $V = (w^2\times l)/2$ (**1**);

The tumour relative increment rate:

$T/C\ (\%) = T_{RTV}/C_{RTV}\times100\%$ (**2**);

Inhibition of tumour growth:

$IR\ (\%) = (W_c-W_t)/W_c\times100\%$ (**3**)

Where w and l mean the shorter and the longer diameter of the tumour, respectively; T_{RTV} and C_{RTV} was the RTV of treated group and control group respectively. (RTV: relative tumour volume, $RTV = V_t /V_0$); Wt and W_c mean the average tumour weight of complex-treated and vehicle controlled group respectively.

Acknowledgements

This work was supported by Natural Science Foundation of China (Nos. 81473102, 21271051, 21431001), National Basic Research Program of China (No. 2012CB723501), IRT1225, CMEMR2012-A22 and Natural Science Foundation of Guangxi Province of China (No. 2012GXNSFDA385001) as well as Bagui Scholar Program of Guangxi, China.

Conflict of interest

The authors declare no conflict of interest.

Notes and references

[a] *State Key Laboratory Cultivation Base for the Chemistry and Molecular Engineering of Medicinal Resources, School of Chemistry & Pharmacy, Guangxi Normal University, Guilin 541004, China. Fax: +86(0)773-2120958. Tel: +086-773-2120998, E-mail: chenzf@gxnu.edu.cn (Z.-F. Chen), hliang@gxnu.edu.cn (H. Liang).*

† Electronic Supplementary Information (ESI) available: The crystal data, ESI-MS, HPLC, cell cycle analysis, confocal microscope to detect DNA fragmentation, the quenching constants (K_q) of OG and complex **2**, ^1H and ^{13}C NMR for complex **1**. See DOI: 10.1039/b000000x/

‡ The CCDC reference numbers are 1009609, 1009610 for complexes **1** and **2**.

(1) Bruijnincxm, P. C.A.; Sadler, P.J. *Curr .Opin. Chem. Biol.* 2008, *12*, 197–206.
(2) Sun Raymond W.Y.; Ma, D.L.; Wong Ella L.M.; Che, C.M. *Dalton Trans.* 2007, 4884–4892.
(3) Meggers, E. *Chem. Commun.* 2009, 1001–1010.
(4) Gasser, G.; Ott, I.; Nolte, N.M. *J. Med. Chem.* 2011, **54**, 3–25.
(5) Kwong, W.L.; Sun raymond, W.Y.; Lok, C.N.; Siu, F.M.; Wong, S.Y.; Low, K.H.; Che, C. M. *Chem. Sci.* 2013, **4**, 747–754.
(6) Kostova, I.; Trendafilova, N.; Momekov, G. *J. Trace Elem. Med. Biol.* 2008, **22**, 100–111.
(7) Kostova, I.; Momekov, G.; Stancheva, P. *Meta-Based Drugs* 2007, **15925**, 1–8.
(8) Wang, L.; Li W. J.; Song Y.M. *RSC Adv.* 2014, **4**, 42285 –42292.
(9) Chen, Z.F.; Gu, Y.Q.; Song, X.Y.; Liu, Y.C.; Peng, Y.; Liang, H. *Eur. J. Med. Chem.* 2013, **59**, 194–202.
(10) Chen, Z.F.; Wei, J.H.; Liu, Y.C.; Liu, M.; Gu, Y.Q.; Huang, K.B.; Wang, M.; Liang, H. *Eur. J. Med. Chem.* 2013, **68**, 454–462.
(11) Weber, M.L. *Cancer Lett.* 2013, **332**, 304–312.
(12) Ho, Y.P.; To-Kenneth, K.W.; Au-Yeung Steve C.F.; Wang, X.N.; Lin, G. *J. Med. Chem.* 2001, **44**, 2065–2068.
(13) Chen, Z.F.; Liang, H. *Anti-Cancer Agents Med. Chem.* 2010, **12**, 412−423.
(14) Chen, Z.F.; Shi, Y.F.; Liu, Y.C.; Hong, X.; Gen, B.; Peng, Y.; Liang, H. *Inorg. Chem*. 2012, **51**, 1998−2009.
(15) Chen, Z.F.; Liu, Y.C.; Peng, Y.; Hong, X.; Wang, H.H.; Zhang, M.M.; Liang, H. *J . Biol. Inorg. Chem.* 2012, **17**, 247–261.
(16) Wu, Y.C.; Liou, Y.F.; Lu, S.T.; Chen, C.H.; Chang, J.J.; Lee, K.H. *Planta. Med.* 1989, **55**, 163−165.
(17) Chen, S.B.; Gao, G.Y.; Yu, S.C.; Xiao, P.G. *Planta. Med.* 2002, **68**, 554−556.
(18) Chang, F.R..; Hsieh, T.J.; Huang, T.L.; Chen, C.Y.; Kuo, R.Y.; Chang, Y.C. *J .Nat. Prod.* 2002, **65**, 255−258.
(19) Sun, J.; Blaskovich, M.; Knowles, D.; Qian, Y.; Ohkanda, J.; Bailey, R.; Hamilton, A.; Sebti, S. *Cancer Res.* 1999, **59**, 4919−4926.
(20) Wang, Y.; Xiao, J.; Zhou, H.P.; Yang, S.L.; Wu, X.P.; Liang, G.A. *J. Med. Chem* .2011, **54**, 3768−3778.
(21) Palanimuthu, D.; Shinde, S.V.; Somasundaram, K.; Samuelson, A.G. *J. Med .Chem.* 2013, **56**, 722−734.
(22) Canelón, I.R.; Pizarro, A.M.; Habtemariam, A.; Sadler, P.J. *Metallomics* 2012, **4**, 1271−1279.
(23) Teis, D.; Huber, L.D. *Cell Mol. Life Sci.* 2003, **60**, 2020−2033.
(24) Canelón, I.R.; Salassa, L.; Sadler, P.J. *J. Med. Chem.* 2013, **56**, 1291−1300.
(25) Deubel, D.V.; Lau-Justin, K.C. *Chem. Commun.* 2006, 2451−2453.
(26) Husain, A.; Yan, X.J.; Rosales, N.; Aghajanian, C.; Schwartz, G.K.; Spriggs, D.R.; *Clin. Cancer Res*. 1997, **3**, 2089–2097.
(27) Rodriguez, R.; Miller, K.M.; Forment, J.V.; Bradshaw, C.R.; Nikan, M.; Britton, S.; Oelschlaegel, T.; Xhemalce, B.; Balasubramanian, S.; Jackson, S. P. *Nat. Chem. Biol.* 2012, **8**(3), 301–310.
(28) Chtchigrovsky, M.; Eloy, L.; Jullien, H.; Saker, L.; Bendirdjian, E.S.; Poupon, J. *J. Med. Chem.* 2013, **56**, 2074–2086.
(29) Hamelik, R.M.; Krishan, A. *Cytometry Part A* 2009, **75A**, 862–865.
(30) Kang, M.H.; Reynolds, C.P. *Clin. Cancer Res.* 2009, **15**, 1126–1132.
(31) Soldani, C.; Scovassi, A.I. *Apoptosis* 2002, **7**, 321–328.
(32) Brunelle, J.K.; Letai, A. *J. Cell Sci*. 2009, **122**, 437–441.
(33) Wang, C.H.; Shih, W.C.; Chang, H.C.; Kuo, Y.Y.; Hung, W.C.; Ong, T.G.; Li, W. S. *J. Med. Chem.* 2011, **54**, 5245−5249.
(34) http://ww.biotium.com/product/product_types/Nucleic_A/price _and _info.asp? item=41003 &layer1=09;&layer2=09A.
(35) Otero, L.; Vieites, M.;,Boiani, L.; Denicola, A.; Rigol, C.; Opazo, L.; Opazo, L.; Olea-Azar, C.; Maya, J. D.; Morello, A.; Krauth-Siegel, R. L.; Piro, O. E.; Castellano, E.; Gonzalez, M.; Gambino, D.; Cerecetto, H. *J .Med. Chem* .2006, **49**, 3322–3331.
(36) Satyanarayana, S.; Dabroniak, J.C.; Chaires, J.B. *Biochemistry* 1992, **31**, 9319–9324.
(37) Dhar, S.; Nethaji, M.; Chakravarty, A.R. *Inorg. Chem.* 2005, **44**, 8876−8883.
(38) Chen, Z.F.; Tan, M.X.; Liu, Y.C.; Peng, Y.; Wang, H.H.; Liu, H.G.; Liang, H. *J. Inorg. Biochem.* 2011, **105**, 426–434.
(39) Barton, J.K.; Dannenberg, J.J. *J. Am. Chem. Soc.* 1982, **104**, 4967–4969.
(40) Silva, P.P.; Guerra, W.; Silveira, J.N.; Ferreira-Ana, M.C.; Bortolotto, T.; Fischer, F.L.; Terenzi, H.; Neves, A.; Pereira-Maia, E. C. *Inorg .Chem.* 2011, **50**, 6414–6424.
(41) Boutros, R.; Lobjois, V.; Ducommun, B. *Nat. Rev. Cancer* 2007, **7**, 495–507.
(42) Skladanowski, A.; Bozko, P.; Sabisz, M.; *Chem. Rev.* 2009, **109**, 2951–2973.
(43) Chen, Z.F.; Tan, M.X.; Liu, L.M.; Liu, Y.C.; Wang, H.S.; Yang, B., Peng, Y.; Liu, H.G.; Liang, H.; Orvig, C. *Dalton Trans.* 2009, 10824–10833.
(44) Hsu, J.L.; Ho, Y.F.; Li, T.K.; Chen, C.S.; Hsu, L.C.; Guh, J.H. *Biochem. Pharmacol*. 2012, **84**, 59–67.
(45) Liu, Y.C.; Chen, Z.F.; Liu, L.M.; Peng, Y.; Hong, X.; Yang, B.; Liu, H. G.; Liang, H.; Orvig, C. *Dalton Trans*. 2009, 10813−10823.
(46) Wu, N.; Wu, X.W.; Agama, K.; Pommier, Y.; Du, J.; Li, D.; Gu, L.Q.; Huang, Z.S.; An, L.K. *Biochemistry* 2010, **49**, 10131−10136.
(47) Koo-Otilia, M.Y.; Rubinstein, I.; Önyüksel, H. *Pharm. Res.* 2011, **28**, 776–787.
(48) Rackham, O.; Nichols, S.J.; Leedman, P.J.; Berners-Price, S.J.; Filipovaka, A. *Biochem. Pharmacol*. 2007, **74**, 992–1002.
(49) Liu, Z.; Habtemariam, A.; Pizarro, A.M.; Fletcher. S.; Kisova. A.; Vrana. O.; Vrana, O.; Salassa, L.; Bruijnincx, P.C. A.; Clarkson, Guy J.; Brabec, V.; Sadler, P. J. *J. Med. Chem.* 2011, **54**, 3011–3026.
(50) Castonguay, A.; Doucet, C.; Juhas, M.; Maysinger, D. *J. Med. Chem.*2012, **55**, 8799−8806.
(51) Zhang, J.J.; Sun Raymond, W.Y.; Che, C.M. *Chem. Commun*. 2012, **48**, 3388–3390.
(52) Roos, W.P.; Kaina, B. *Cancer Lett*. 2013, **332**, 237–248.
(53) Capranico, G.; Marinello, J.; Baranello, L. *Biochim. Biophys. Acta Reviews on Cancer* 2010, **1806(2)**, 240–250.
(54) Yan, J.J.; Chow-Andy, L.F.; Leung, C.H.; Sun Raymond, W.Y.; Ma, D.L.; Che, C.M. *Chem. Commun.* 2010, **46**, 3893–3895.
(55) Tan, C. P.; Lai, S.S.; Wu, S.H.; Hu, S.; Zhou, L.J.; Chen, Y.; Wang, M.X.; Zhu, Y.P.; Lian, W.; Peng, W.L.; Ji, L.N.; Xu, A.L. *J. Med. Chem.* 2010, **53**, 7613–7624.
(56) Beck, D. E.; Agama, K.; Marchand, C.; Chergui, A.; Pommier, Y.; Cushman, M. *J. Med .Chem.,* 2014, **57**, 1495−1512.

Water-soluble oxoglaucine-Y(III), Dy(III) complexes: In vitro and in vivo anticancer activity by triggering DNA damage, leading to S phase arrest and apoptosis

Jian-Hua Wei, Zhen-Feng Chen,* Jiao-Lan Qin, Yan-Cheng Liu, Zhu-Quan Li, Taj-Malook Khan, Meng Wang, Yan-Hua Jiang, Wen-Ying Shen and Hong Liang*

Water-soluble oxoglaucine-Y(III), Dy(III) complexes were synthesized and characterized. They exhibited considerable in vitro anticancer activity. Dy(III) complex can trigger DNA damage in HepG2 cells, resulting in a cell cycle arrest in S phase and leading to cell apoptosis. The S phase cell-cycle arrest is caused via an ATM (ataxia-telangiectasia mutated)-Chk2-Cdc25A pathway. Dy(III) complex effectively inhibited tumor growth in the BEL-7402 xenograft mouse model, and exhibited higher safety in vivo than cisplatin.